Synergistic effect of water-soluble species and relative humidity on morphological changes of aerosol particles in Beijing mega-city during severe pollution episodes

Xiaole PAN[1], Baozhu GE[1], Zhe WANG[1,2], Yu TIAN[1,3], Hang LIU[1,3], Lianfang WEI[1], Siyao YUE[1,3], Itsushi UNO[2], Hiroshi KOBAYASHI[4], Tomoaki NISHIZAWA[5], Atsushi SHIMIZU[5], Pingqing FU[1,3,7], Zifa WANG[1,3,6],

[1] State Key Laboratory of Atmospheric Boundary Layer Physics and Atmospheric Chemistry, Institute of Atmospheric Physics, Chinese Academy of Sciences, Beijing, 100029, China

[2] Research Institute for Applied Mechanics, Kyushu University, Kasuga, 816-8580, Japan

[3] University of Chinese Academy of Sciences, Beijing,100049, China

[4] University of Yamanashi, Yamanashi, 400–0016, Japan.

[5] National Institute for Environmental Studies, Ibaraki, 305-8506, Japan

[6] Center for Excellence in Regional Atmospheric Environment, Institute of Urban Environment, Chinese Academy of Sciences, Xiamen 361021, China

[7] Institute of Surface-Earth System Science, Tianjin University, Tianjin, 300072, China

Correspondence to: Xiaole PAN (panxiaole@mail.iap.ac.cn)

Abstract. Depolarization ratio (δ) of backscattered light is an applicable parameter for real-time distinguishing sphericity of particle, which has been widely adopted by ground-based Lidar observation. In this study, δ value of particles and chemical compositions in both $PM_{2.5}$ (aerodynamic diameter less than 2.5μm) and PM_{10} (aerodynamic diameter less than 10 μm) were concurrently measured on the basis of a bench-top optical particle counter with a polarization detection module (POPC) and a continuous dichotomous Aerosol Chemical Speciation Analyzer (ACSA-14) from November 2016 to February 2017 at an urban site in Beijing mega city. In general, measured δ value depended on both size and sphericity of the particles. During observation period mass concentration of NO_3^- in $PM_{2.5}$ (fNO_3) was about an order of magnitude higher than that in $PM_{2.5-10}$ (cNO_3) with a mean fNO_3/cNO_3 ratio of 14 ± 10. Relative low fNO_3/cNO_3 ratio (~5) was also observed under higher relative humidity condition, mostly due to heterogeneous processes and particles in the coarse mode. We found that δ value of ambient particles in both $PM_{2.5}$ and $PM_{2.5-10}$ obviously decreased as mass concentration of water-soluble species increased at

unfavorable meteorological condition. It indicated that morphology of particles was changed as a result of water-absorbing processes. The particles with Dp = 5 μm were used to represent mineral dust particles, and its δ values ($\delta_{Dp=5}$) decreased by 50% as mass fraction of cNO$_3$ increased from 2% to 8% and ambient relative humidity increased up to 80%, suggesting that mineral dust particles were likely to be spherical during humid pollution episode. During the observation, relative humidity inside the POPC measuring chamber was stable at 34 ± 2%, lower than that in ambient condition. Its influence on the morphology was estimated to be limited and did not change our major conclusion. This study highlights the evident alteration of non-sphericity of mineral dust particles during their transport owing to synergistic effect of both pollutant coatings and hygroscopic processes which play an important role in evaluation of its environmental effect.

1 Introduction

Tropospheric aerosols, in particular the particles with aerodynamic diameter less than 2.5 μm (PM$_{2.5}$), have detrimental impact on human health(Zheng et al., 2015). It degrades the air quality by increasing atmospheric turbidity, and affects regional/global climate by disturbing the solar radiation transfer in the Earth system via scattering/absorbing light directly and altering amount and lifespan of cloud (Ramanathan et al., 2001;Kaufman et al., 2002). In the past decades, intensive anthropogenic/industrial activities in East Asia emitted huge amount of primary pollutants such as SO$_2$, NO$_x$, NH$_3$, VOCs etc., which resulted in severe air pollution. PM$_{2.5}$ was mainly composed of light-scattering species (sulfate, nitrate, ammonium, organics etc.) and light-absorbing matter (BC, BrC etc.). Under high relative humidity condition, most of aerosol particles absorb water vapor and undergo apparently hygroscopic growth, which lead to dramatic changes in its mass concentration, size distribution, optical properties (single scattering albedo etc.), as well as its corresponding morphologies (Li et al., 2017).

Mineral aerosol is also one of the key compounds in East Asia, it was frequently reported to be coated by anthropogenic pollutants along its transport owing to heterogeneous reactions with reactive acidic gas and coagulation of soluble particles. In polluted area, photo-chemically formatted nitric acid (HNO$_3$) could easily react with CaCO$_3$ to form Ca(NO$_3$)$_2$ on the surface of dust particles. The consecutive water-absorbing process will also lead to apparent morphological changes of dust particles (Krueger et al., 2003;Laskin et al., 2005;Tang et al., 2016), which also impact on dust-cloud interaction (Sullivan et al., 2009;Tang et al., 2015) and new particle formation etc. Till now, online investigation on the morphological changes of aerosol particle in the ambient environment is still limit. The widely-adopted method to study the morphology and mixing state of particles is filter-based single particle sampling with electron-microscopy inspection in laboratory. For example, scanning electron microscopy (SEM) coupled with energy dispersive X-ray spectrometry (EDX) could provide information about surface topography, composition of the sample surface by scanning it with a high-energy beam of electrons. Li and Shao (2009) using Transmission electron microscopy (TEM) found that approximate 90% of sampled mineral particles were covered by visible coatings during pollution episode in Central East China. As a matter of fact, such hygroscopic coating on some individual dust particles was observed not only in polluted area but also at clean marine area. The observation on R/V during ACE-Asia found that dust particles mixed with chloride was sometimes dominant over sulphate and nitrate due to disassociation of acidified sea salt particles (Sullivan et al., 2007). Tobo et al. (2010) found that Asian dust particles could

2

61 also be deliquescent to aqueous droplet as a result of formation of $CaCl_2$. Dust particle could also acquire sulfate coatings via

62 either heterogeneous uptake of gaseous SO_2 and subsequent oxidation or coagulation within cloud or fog droplets (Kojima et

63 al., 2006), as well as volatile carbonaceous species due to condensation processes (Kim and Park, 2012). Although diversity

64 in chemical composition and structure of single particles with different degree of aging were investigated in the past studies,

65 these analyses had to be inspected subjectively one by ones, and such labor-intensive operation cause difficult in broadening

66 the results due to poor statistics(Li and Shao, 2009;Li et al., 2017).

67 To obtain better understanding the real-time morphological variation of atmospheric processing particles, polarization

68 property of backscattering light from the illuminated particle has been used as an applicable surrogate. For spherical particle,

69 oscillation direction of magnetic wave of scattering light was identical to the incident light. Therefore, depolarization ratio

70 (DR, here defined as the ratio of *s*-polarized to *p*-polarized backward component) was zero theoretically. However, for

71 uncoated dust particles, the direction deviates significantly with a large DR value. Such characteristic is widely used to

72 distinguish dust and spherical particles by both ground-based Lidar observation (Asian Dust and Aerosol Lidar Observation

73 Network, AD-Net) (Shimizu et al., 2016) and satellite on-board remote sensing (Cloud-Aerosol Lidar with Orthogonal

74 Polarization on-board the CALIPSO) (Winker et al., 2009;Zhang et al., 2018) presuming that spherical particles and dust were

75 externally mixed. On the basis of this technique, studies on spatial-resolved distribution (Hara et al., 2008;Uno et al., 2008),

76 transport pattern (Uno et al., 2009) of pollution and dust, and data processing algorithm (Nishizawa et al., 2007;Nishizawa et

77 al., 2011;Winker et al., 2009) have been widely performed. For instance, Shimizu et al. (2004) summarized the contributions

78 of different aerosol types on the total backscattering coefficient at multiple sites in East Asia using three-channel Mie scatting

79 Lidar data. Huang et al. (2015) identified anthropogenic dust particles due to human activities and its contribution to global

80 dust loading on the basis of CALIPSO observation. Recently, a multi-wavelength Mie-Raman Lidar (MMRL) and a new

81 algorithm were developed to estimate extinction coefficients for black carbon, dust, sea salt, and air-pollution aerosols (a

82 mixture of sulfate, nitrate and organic carbon substances)(Hara et al., 2017;Nishizawa et al., 2017).

83 Once the dust particles were coated by other water-soluble pollutants, its polarization degree altered. Till now, it is still a

84 challenge to real-time classifying in coated/uncoated dust particles according to its morphological changes. In particular, Lidar

85 adopted a volume depolarization ratio to discriminate different aerosol types; it was easily biased due to presence of small

86 spherical particles in the volume of targeted air volume. To overcome this shortcoming, recently a bench-top optical particle

87 counter equipped with a depolarization module (Polarization Optical Particle Counter) was developed to detect the size-

88 resolved polarization of individual particles. POPC is capable of investigating the temporal variation of mixing state of single

89 dust particles. The observation at an urban site in Japan showed that DR of super-micron particles decreased evidently due to

90 an increase of mass fraction of nitrate concentration during a long stagnant dust event (Pan et al., 2015). In Beijing,

91 sphericalized dust particles were observed during a typical dust even at high relative humidity condition (Wang et al., 2017;Pan

92 et al., 2017). The long-term comprehensive observation on such effect was still lacking.

93 From November 15, 2016 to Februarys 18, 2017, Beijing consecutively suffered from several severe air pollutions with hourly

averaged mass concentration of PM$_{2.5}$ and PM$_{2.5-10}$ larger than 300 μg/m^3 and 100 μg/m^3. It provided a good chance to investigate into the interaction between dust particles with pollutants. During this period, chemical composition, size distribution, polarization properties of aerosol particles were concurrently measured, as well as vertical profile of backscattering coefficient by Lidar at a downtown tower site of Beijing mega city. The objective of this study was to investigate depolarization properties of aerosol particles in the polluted urban site on the single-particle basis, and to study the impact of both water-soluble species and relative humidity (RH) on the morphological changes of dust particles. This study will provide useful information in better understanding the physical and optical properties of particles in East Asia, and improving numerical simulation on its environment/climate effect.

2 Observations

2.1 Observation overview

The field measurement was performed at a tower campus of Institute of Atmospheric Physics/Chinese Academy of Sciences in the downtown area of Beijing mega city. The observation site located between 3rd North Ring road and 4th North Ring road, where anthropogenic emissions are intensive in the daytime. Within the campus (150 m x 50 m), there is a 325-m tower for meteorological measurement and scientific research; therefore, anthropogenic activity nearby is limited. During the observation period, a continuous dichotomous Aerosol Chemical Speciation Analyzer (ACSA-14) was placed on the roof of two-story building in the campus. Polarization Optical Particle Counter was placed in air-conditioned room on the roof to measure polarization properties of single particle less than 10 μm. To avoid loss of particles in coarse mode, the sampled air was drawn into the room by a supporting pump (flow rate: 10 lpm) through 2 m long 1/4-inch vertically assembled stainless steel tube. From November 15 to December 15 2016, a UK-China joint field campaign, entitle as "In-depth study of air pollution sources and processes within Beijing and its surrounding region (APHH-Beijing)" was also performed in the tower campus. Detailed information about the objectives and instruments are shown in webpage (https://www.atmos-chem-phys.net/special_issue932.html).

2.2 Instruments

In this study, mass concentrations of particulate matter and water-soluble chemical compounds in both PM$_{2.5}$ and PM$_{2.5-10}$ were measured by ACSA-14 (KIMOTO electric Co. Ltd, Osaka, Japan) with 1-hour intervals at the observation site. The mass concentration of particulate matter was determined using beta-ray absorption method. Mass concentration of SO$_4^{2-}$ was determined on the basis of BaSO$_4$-based turbidimetric method with addition of BaCl$_2$ dissolved in polyvinylpyrrolidone solution. Mass concentrations of NO$_3^-$ and water-soluble organic carbon were determined using ultraviolet absorption-photometric method. Because mass concentration of NO$_3^-$ was general high in Beijing, the instrument generally collected aerosol samples in the first 5~10 minute in each hour and analyzed the samples in the rest time to guarantee follow Beer-Lambert Law. The acidity of particles [H$^+$], in unit of nmol/m^3, was semi-quantitatively determined using pH-indicator absorption-photometric method. The basic equation is pH$_{solution}$ = −log [H$^+$ × 10^{-6}+ 10$^{-4.6}$], presuming that all the water-soluble

4

26 matter was dissolved in the extract liquid with pH value of 4.6. A factor of 10^{-6} was used to convert unit of $[H^+]$ from nmol/m^3

27 to mol/L. The comparison of $[H^+]$ in $PM_{2.5}$ between ACSA and off-line filter-pack measurement showed a good linear

28 correlation ($[H^+]_{ACSA} = 3.33 + 0.81 \times [H^+]_{FP}$) with $r^2 = 0.54$ (Personal communication with Prof. Osada in Nagoya University).

29 The details of the ACSA instrument are described in literature (Kimoto et al., 2013).

30 Depolarization ratio (δ) of single particle was determined using a Polarization Optical Particle Counter (POPC). POPC adopted

31 a 780 nm linearly polarized laser beam to illuminate the aerosol particles that passed through measuring chamber vertically.

32 The direction of vibration of the electric field of the incident laser is parallel to the plane of the scattering angle. Detailed

33 information about POPC was described in literatures (Kobayashi et al., 2014;Pan et al., 2016;Pan et al., 2017). Forward

34 scattering signal at 60-degree respect to direction of incident light was measured by a photodiode with acceptance angle of

35 45-degree to determine the size of particle. The backward scattering signal at 120 degree was split into P component (parallel

36 with respect to the plane of the scattering angle) and S component (perpendicular with respect to the plane of the scattering

37 angle). Herein, the depolarization ratio (parallel with respect to the plane of the scattering angle) of the particles was defined

38 as the ratio of S component to P component (S/P). To avoid the coincidence error of the measurements, the inlet flow rate of

39 POPC was set to 80 cubic centimeters per minute (ccm) and was diluted with zero air (920 ccm). During measurement, the

40 temperature and relative humidity inside measuring chamber were stable at 29.2 ± 0.1 ℃ and 34.3 ± 1.6 %, respectively.

41 Overall measurement uncertainty in size determination was less than 15%.

42 During observation period, the vertical structure of backscattering coefficient for aerosols was derived from Mie-scattering

43 Lidar system that installed at the same place of ACSA-14. This Lidar system, developed by the research group in National

44 Institute for Environmental Studies (NIES), employs a flash-lamp-pumped Q-switching Nd:YAG laser as the light source. It

45 emits pulsed lights with wavelength of 1064 nm and 532 nm with at a frequency of 10 Hz, and collects the backscattered light

46 from the atmosphere by a 20 cm Schmidt-Cassegrain telescope. The light at 532-nm wavelength is also further separated into

47 S and P component (Sugimoto et al., 2002). The algorithm for classifying sphere and dust particles was described in literatures

48 (Shimizu et al., 2017;Nishizawa et al., 2011). To be noted that, direct comparison of depolarization ratio between POPC and

49 Lidar system was difficult. Firstly, Lidar system receives backscattering light at almost 180 degree with a field of view of 1

50 mrad; whereas POPC employs 120-degree backscattering signal. Secondly, Lidar system measures the total volume

51 depolarization from a volume of targeted air parcel; whereas depolarization properties from POPC is on a single particles

52 basis.

2.3 Footprint analysis

54 We simulated footprint region of aerosol particles at the observation site using NOAA Hybrid Single Particle Lagrangian

55 Integrated Trajectory (HYSPLIT) model (v4.9; available at http://ready.arl.noaa. gov/HYSPLIT.php). This model has been

56 widely applied into calculating long-range or meso-scales transport and footprint regions of air pollutions with fast

57 computational speed and high spatial resolution. HYPLIT model is capable of forward/backward run in time to simulate the

dispersion/potential source of tracers in a given location. Detailed description and validations of this model was shown in webpage. In this study, input meteorological data of model is the product (GDAS dataset) of Global Forecast System (GFS) from National Centers for Environmental Prediction (NCEP) with a spatial resolution of 0.5 by 0.5 degree, and a time-resolution of 3 hours (0000, 0600, 1200 and 1800 UTC from data assimilation product; 0300, 0900, 1500 and 2100 UTC from forecast model). By offsetting the release point by a meteorological grid point in the horizontal and 0.01 sigma units in the vertical, ensemble simulation have 27 trajectories were calculated simultaneously in each hour, providing great advantage in evaluate the uncertainty and potential footprint region. In the present study, the grids at which height of backward endpoint of air parcel was less than the height of mixing layer were labeled as potential footprint region.

3 Results and discussions

3.1 Overview in particulate matters and chemical species

3.1.1 Comparison of mass concentration of particulate matters

Figure 2a shows the temporal variations of mass concentrations of ambient $PM_{2.5}$ that were measured by ACSA-14 at the observation site. For comparison, mass concentration of $PM_{2.5}$ observed at a state-controlled monitoring station (Olympic Centre, about 3 km northeast of the LAPC site) was plotted in the figure. In general, two results were in good consistence with $r^2 = 0.8$, indicating that the pollution events were generally in regional scale with minor interference from emission sources nearby. During observation period, number size distribution of ambient particles with optical diameter between 0.3 μm - 10 μm were measured with POPC, and the mass concentration of $PM_{2.5}$ was estimated assuming that all the particles were spherical with a density of 1.77 g/cm^3. Mass concentration of $PM_{2.5}$ estimated by POPC was compared well with ACSA-14 measurement before January 7, 2017, when ambient relative humidity (RH) was almost above 40%. Whereas estimated mass concentration of $PM_{2.5}$ was underestimated obviously. One possible explanation is that, both air temperature and ambient RH after January 7, 2017 decreased evidently. The interaction between water-soluble matters in $PM_{2.5}$ and moisture were unlikely occurs, and the hypothesis of spherical shape of particles due to hygroscopic may resulted in relatively larger uncertainty in estimating the optical size of particle on the basis of scattering light. Another possibility is that the chemical composition of particles was different (section 3.1.2). As shown in Figure 2d, the northerly wind become stronger, which resulted in larger proportion of mineral dust matters, the latter which have larger density (2.2 - 2.8 g/cm^3). Deploying the same density for both particle in fine mode and coarse mode will lead to underestimation of total mass. It was pronounced for the case in January 29, 2017 that observation site was subject to floating dust event with a hourly averaged mass concentration of PM_{10} reached 734 μg/m^3. Daily averaged mass concentration of $PM_{2.5}$ measured by ACSA-14 was 354.3 μg/m^3, four times higher than the values (77.1 μg/cm^3) estimated by POPC. Deployment of a larger particle's density of 2.8 g/cm^3 only explain 35% of the difference. Low detection limit of particle size of POPC was 0.5 μm, and miscounting of particles less than 0.5 μm was estimated to contribute another 10% of the difference. The most possible reason is that the irregularity of particles in fine mode resulted in significant underestimating in particle diameter on the basis of scattering signal. However, the estimation of

spherical particles diameter by POPC bears smaller bias theoretically. For example, during a typical anthropogenic pollutant dominant case on January 1, 2017, mass concentrations of $PM_{2.5}$ and PM_{10} was as high as 438.8 and 626.2 μg/m^3, respectively. Hourly averaged mass concentration of $PM_{2.5}$ estimated by POPC correlated well with ACSA-14 measurement with a ratio of 1.1 ± 0.1. It was noticeable that $PM_{2.5}$ accounted for 80% of PM_{10}, and ambient relative humidity was 65%. It implied that anthropogenic water-soluble compounds in $PM_{2.5}$ underwent hygroscopic processes that may alter non-sphericity of the particles (section 3.5).

Regarding the particles in coarse mode, mass concentration estimated by POPC is much better than that in fine mode. It was because, firstly, the detection efficiency of POPC for the particles in coarse mode was better than that in fine mode, and miscounting of particles in coarse mode by POPC was less likely to occur; secondly, interference of non-sphericity of particles in coarse mode was insignificant in determining size of particle according to scattering signal. Besides, change in the refractive index of particles due to mixing of mineral dust particles with anthropogenic pollutants (such as black carbon) also have limited impact in size determination. In general, daily averaged mass fraction of $PM_{2.5-10}$ in PM_{10} ($PM_{2.5-10}/PM_{10}$) was ranging 0.25 ~ 0.7 (Supplementary Figure). The minimum value occurred in severe pollution days when daily averaged mass concentration of $PM_{2.5}$ was larger than 250 μg/cm^3 (Air Quality Level: VI), whereas $PM_{2.5-10}/PM_{10}$ ratio increased as mass concentration of $PM_{2.5}$ decrease. It was because formation of secondary particulate matters (such as sulfate and nitrate) during pollution episode was so overwhelming that make the contribution of mineral dust decrease, although mass concentration of $PM_{2.5-10}$ increased. A number of studies have addressed the importance of mineral dust in promoting new particle formation (Nie et al., 2014) and conversion of SO_2 to sulfate (He et al., 2014), both of which was related to formation of OH radical. However, this study was performed in winter, role of mineral dust in the formation of regional pollution is out of scope of this study.

3.1.2 Chemical compounds in fine and coarse mode

In winter, nitrate, sulfate and water-soluble organic carbon (WSOC) were found in both fine mode and coarse mode (Figure 3). Mass concentration of nitrate in the fine (fNO_3) was 28.3 ± 33.7 μg/m^3 averagely with a maximum value of 190.9 μg/m^3. Mass concentration of nitrate in the coarse mode (cNO_3) was 2.9 ± 4.8 μg/m^3. The maximum value of cNO_3 (43.1 μg/m^3) occurred at the different time from that for fNO_3, implying of complicated mass equilibrium of nitrate among different size range. Table 1 summarizes the fNO_3/cNO_3 ratio as a function of mass concentration of $PM_{2.5}$ at RH > 40% and RH < 40%. We found that, when ambient RH was less than 40%, fNO_3/cNO_3 ratio has a positive correlation with mass concentration of $PM_{2.5}$, which demonstrated that nitrate mass preferentially formed in fine mode and mass transfer of nitrate toward coarse mode was unlikely happen due to hygroscopic processes of particles; However, when ambient RH was larger than 40%, fNO_3/cNO_3 ratio did not increase with $PM_{2.5}$ concentration with a mean of 12.4 ± 6.5. The possible explanations were, first, once the aerosol phase nitrate formed in the fine mode, it absorbed water vapor simultaneously and grew larger; secondary, ambient nitric acid may directly stick on the surface of particles in coarse mode through heterogeneous processes; Although

high concentration of $PM_{2.5}$ in Beijing was regard as synergistic contributions from both local formation and long-range transport, it did not influence the fNO_3/cNO_3 ratio apparently, at least in the present study.

Mass concentration of sulfate in the fine mode (fSO_4) and in the coarse mode (cSO_4) were 18.9 ± 24.8 µg/m^3 and 2.2 ± 2.5 µg/m^3 with maximum values of 143.1 µg/m^3 and 25.2 µg/m^3, respectively. As shown in Figure 3b, the variabilities of fSO_4 and cSO_4 concentrations generally have the same trend. fSO_4/cSO_4 ratio increased with mass concentration of $PM_{2.5}$, irrespective of ambient RH. The positive correlation between fSO_4/cSO_4 ratio and RH indicated that water vapor also took effect in the formation of sulfate. It was worthy to note that, fNO_3/fSO_4 ratio varied among cases due to different air mass origin and meteorology condition. For instance, on Dec 21, 2016 (blue shaded strip in Figure 3), mass concentration of fNO_3 and fSO_4 were 122.4 µg/m^3 and 74.1 µg/m^3, with a fNO_3/fSO_4 ratio of 1.6; however on Jan 1, 2017 (red shaded strip in Figure 3), mass concentration of fSO_4 increased to 125.2 µg/m^3 and fNO_3 decreased to 99.2 µg/m^3 with a fNO3/fSO4 ratio of 0.79. Backward trajectory analysis for the case on Jan 1, 2017 showed that the air mass was mainly transport from North China Plain along Taihang Maintain, fossil fuel usage in NCP in winter mainly contribute to the sharp increase of fSO_4; however, for the case on Dec 21, 2016, the air mass was mostly stagnant near Beijing area, and the intensive emission of NO_x resulted in the large difference between fNO_3 and fSO_4. The variability of WSOC in both fine mode (fWSOC) and coarse mode (cWSOC) were consistent with fSO_4 with maximum values of 167.6 µg/m^3 and 8.7 µg/m^3 (Figure 3c).

Mass fraction of total water soluble matters (WSM) in $PM_{2.5}$ and acidity of the particle are shown in Figure 3d. Here, WSM includes only SO_4^{2-}, NO_3^-, WSOC, and NH_4^+, the latter of which was estimated on the basis of equation ($[NH_4^+] = 18 \times ([SO_4^{2-}]/96 \times 2 + [NO_3^-]/62 \times 2 - [H^+]/1000)$. In general, mass fraction of WSM in $PM_{2.5}$ during pollution period was higher than that during clean period. On average, WSM/$PM_{2.5}$ was 0.5 ± 0.16. We found that, WSM/$PM_{2.5}$ was more likely related to origin and residence time of air mass than the ambient loading of $PM_{2.5}$ concentration. For example, daily averaged mass concentration of $PM_{2.5}$ reached the maximum (447.5 µg/m^3) on Jan 1, 2017; whereas maximum value of WSM/$PM_{2.5}$ (0.80) occurred on Jan 7, 2017 when the pollution period almost ended. On Jan 1, 2017 observation site was prevailing southwesterly wind which introduced pollutants from NCP where industrial emission was intensive; However, air mass was mostly from east region on Jan 7, 2017, and high concentration of cNO_3 (Figure 3a) and high RH (Figure 2d) indicated that heterogeneous processes played a key role. Mole concentration of $[H^+]$ in fine mode (fH^+) correlated well with mass concentration of fSO_4 (Figure 3d), implying of possibility of presence of surplus of sulfuric acid that converted from SO_2 that emitted from coal burning during heating period.

Table 1 The relationship between fNO_3/cNO_3, fSO_4/cSO_4 and mass concentration of $PM_{2.5}$ at different RH condition.

RH Classification	PM$_{2.5}$ Classification (µg/m^3)	PM$_{2.5}$ (µg/m^3)		fNO3/cNO3 (unitless)		fSO4/cSO4 (unitless)		RH (%)	
		Avg.	S.D.	Avg.	S.D.	Avg.	S.D.	Avg.	S.D.
RH<40%	<25	16.3	6.3	12.5	6.8	3.6	2.2	29.3	4.7

8

	25-50	37.5	7.2	15.1	7.2	4.7	1.9	32.3	5.9
	50-75	59.9	7.8	17.5	8.5	5.6	1.8	33.4	6.8
	>75	98.2	23.4	26.2	12.1	6.2	1.8	32.2	6.4
	<50	33.4	13.1	12.1	6.1	4.5	1.8	53.3	14.1
	50-100	82.1	8.3	13.0	9.6	5.6	2.3	54.4	10.6
RH>40%	100-150	119.2	14.5	9.5	5.3	6.1	3.4	60.2	10.1
	150-200	175.6	14.5	12.9	5.9	7.8	2.7	59.8	6.8
	>200	290.9	61.6	14.3	5.3	10.3	2.0	61.1	9.2

3.2 Volume size distribution and depolarization ratio

Volume size distribution of aerosols and averaged depolarization ratio (δ) during observation period are shown in Figure 4. In general, evolution of all the pollution cases were well captured by POPC. Volume size distribution of aerosols showed a pronounced peak at 1 μm, at which secondary anthropogenic pollutants were dominant. Correspondingly, δ value of particles were normally less than 0.1, consistent with the previous study in East Asia (Pan et al., 2016). On Nov 19, 2016, two peaks were observed at size range of 1 μm and 2~3 μm. δ value of particles at two size were as low as 0.1. Such pattern of volume size distribution has been described in previous studies (Pan et al., 2015;Pan et al., 2016), which classified such phenomena as a mixing pollution type that both anthropogenic pollutants and mineral dust particles interacted. Five-day trajectory analysis indicated that air mass mainly originated from Mongolia Plateau and they were stagnant over East China for days. Volume peak at size of 4~5 μm was not observed probably due to fast gravity settling of large particles in coarse mode during their stagnancy. On Nov 26, 2016, the observation site was influenced by floating dust, and volume size distribution had a pronounced peak at 4 ~ 5 μm, as expected. δ value of submicron particles also increased to 0.3, implying of the substantial presence of irregular mineral particles in the fine mode. From Dec 30, 2016 to Jan 8, 2017, it had a long-lasting pollution period in Beijing. Volume size distribution of aerosols varied due to impacts from both change in Planet Boundary Layer height and origin of aerosols. Multi-peak fitting analysis indicated that volume size distribution had two peaks with a dominant peak at size of 0.9 μm and another peak at size of 2 μm. Different from case on Nov 19, 2016, the δ values of particles were 0.2~0.4, though ambient RH was the same (> 60%). It implied that chemo-physical properties of the particles were different, probably due to impact by mineral dust. Detailed discussion was in section 3.3.2.

3.3 Variability of δ value for particles of different size

3.3.1 δ value for particles in fine mode

As pointed out in previous study, δ value of particles generally depends on both their size and non-sphericity. Histogram analysis on the particles at size of 1 μm showed that there was one peak mode with δ value of 0.11; For the particles at size of 2 μm, a multi-Gaussian fitting for frequency distribution of δ value showed there were one dominant peak at a value of 0.17 and a shoulder value of 0.23, the latter of which was mostly related to the impact of dust aerosols. We found that variability of δ value of particles in fine mode was a synergistic effect of both water-soluble inorganic matter (WSI) and RH. For example, in Figure 5, δ value of particles at size of 2 μm decreased gradually from 0.3 to 0.1 as mass fraction of WSI in $PM_{2.5}$ increase

9

from 0.2 to 0.65, and RH increased from 38% to 85%. It notes that, δ value of particles in fine mode decreased only when RH > 60% and mass fraction of WSI > 0.6. Mass fractions of both fSO_4 and fNO_3 in $PM_{2.5}$ showed a negative correlation with δ value of the particles at size of 2 μm with a slope of – 0.3 and -0.1, respectively. We speculated that fNO_3 might play a key role in decreasing of δ value of particles in the fine mode because fNO_3 was accounting for ~50% of total WSI and deliquescent point of ammonium nitrate was ~60%, and the impact of ammonium sulfate was less important since it started to undergo hygroscopic growth only at higher RH (79%). Quantitatively distinguishing respective contribution of fNO_3 and fSO_4 on the decrease of δ value of particles was difficult in the present study.

3.3.2 δ value of mineral dust aerosols

Histogram analysis of δ value for the particles at size of 5 μm ($δ_{Dp=5}$) value had a wide range 0.3 - 0.55. Laboratory experiments on typical spherical particles at a size of 5.124 μm (SS-053-P) showed that their $δ_{Dp=5}$ value was 0.07 ± 0.01. The larger $δ_{Dp=5}$ value (> 0.3) of mineral dust particle in the ambient air indicated that they were aspherical in shape. Figure 6 shows time variation of vertical profile of extinction coefficient of dust particles derived from ground-based Lidar observation. We can see that there was a typical dust event on Dec 26, 2016 with a $PM_{2.5-10}/PM_{10}$ ratio of 68%, and extinction coefficient of dust particles at site was larger than 0.3 Km^{-1}. $δ_{Dp=5}$ value of dust particle was varying around 0.5, and no decrease of δ value of dust particles was observed due to low cNO_3 concentration and low RH (Figure 6). Another dust event was from Jan 1, 2017 to Jan 7, 2017, we found that $δ_{Dp=5}$ value of dust particles was apparently low with a mean value of 0.35. In particular, during the period that mass concentration of cNO_3 increased up to 10 μg/m^3 and ambient RH was ranging above 60%, hourly averaged $δ_{Dp=5}$ value of dust particles decreased to 0.2, implying that cNO_3 on the surface of dust particle may form as $Ca(NO_3)_2$ owing to heterogeneous processes, and consecutive hygroscopic growth resulted in the decrease of its $δ_{Dp=5}$ value. Compared with the case on Dec 26, 2016, impact of this dust event was relative weak with a $PM_{2.5-10}/PM_{10}$ ratio of 27%. It was worth noting that all the mineral dust impacting cases were captured by both Lidar and POPC observations, nevertheless, the mixing state of mineral dust particles could be illustrated better with POPC measurement according to their $δ_{Dp=5}$ variations. Once the morphology of mineral dust particles was modified due to cNO_3 coating at high RH condition, Lidar observation may underestimate the impact of dust due to decrease of $δ_{Dp=5}$ value of particles. Such phenomena maybe more likely to happen at the downstream of polluted area. For instance, dust particles were found to be spherical due to interaction with HCl and HNO_3 at marine area (Tobo et al., 2010). Observations using POPC at Kyushu area of Japan also indicated that there was a large number of larger particles with a $δ_{Dp=5}$ value between 0.05 ~ 0.15 when air mass came from NCP of China, implying that the morphology of dust particles were altering with transport (Pan et al., 2016).

3.4 Footprint analysis of mineral dust particles

As discussed above, the decrease of $δ_{Dp=5}$ value of mineral dust particle was influenced by both mass concentration of cNO_3 and ambient RH. We selected two mineral dust-influencing episodes to demonstrate such impact (Figure 7). Here, footprint

10

region of the air mass was calculated for the period that hourly averaged mass concentration of cNO_3 was higher than 5 μg/m^3. For the episode between Nov 24 and Dec 7 2016, the footprint region of air mass covered west of Inner Mongolia province and South of Hebei province. The particles in coarse mode seemed to mostly related with anthropogenic dust (defined as dust aerosols due to human activity, such as agriculture, industrial activity, transportation etc.) in NCP where NO_x emission and atmospheric nitrate loading were also high. Averaged RH was relatively low with a mean value of 30% (Figure 7c). However, for the episode between Jan 1 and Jan 8, 2017, averaged RH within the footprint region around NCP was as high as 60% (Figure 7d), although mineral dust particle had similar origins. Adsorption of water vapour and consecutive heterogeneous reaction lead to obvious decrease of $\delta_{Dp=5}$ value of mineral dust particles. It indicated that a synergetic effect of both nitrate in coarse mode and high RH condition lead to morphological changes in dust shape. The variability of morphological changes was simulated on the basis of T-matrix methodology and randomly oriented elongated ellipsoid particles. We found that observed maximal $\delta_{Dp=5}$ value (0.5) of dust particle corresponded to an aspect ratio (defined as ratio of the longest dimension to its orthogonal width) of 1.7. When δ value of mineral dust particles decrease to 0.2, the aspect ratio was estimated to be 1.5, not being "spherical". Therefore, we considered such dust particles as being 'quasi-spherical'. Huang et al. (2015) pointed out that layer-integrated δ value of anthropogenic dust particles in the PBL of NCP was lower than that of Taklimakan dust on the basis of CALIPSO Lidar measurement, mostly due to mixed with other more spherical aerosol within the PBL. Because Lidar observation just provide an averaged δ value of all the particle in the detecting volume, external mixing of dust particle with substantial amount of secondary anthropogenic particles in spherical shape could also result in a low δ value. From view point of this study, irregularity of anthropogenic dust particles in NCP were possibly the same as the nature dust in the source region, however, their interaction in particular at high RH condition will obviously lead to decrease in δ value.

3.5 Impact of heterogeneous reaction on δ value of particles

As shown in Figure 8, δ value of particles decrease obviously with increase of mass fraction of water soluble Matters (WSM), in particular at high RH condition. For the particles at Dp = 2 μm, their δ value was normally 0.3 when mass fraction of WSM in $PM_{2.5}$ was less than 0.2, whereas it decreased to 0.1 when the mass fraction of WSM increased to 0.6, and RH also increased to 80% (Figure 8a). The linear relation was because the growth of particles in fine mode was closely related to formation of secondary inorganic matters (sulfate, nitrate, etc.) and organic aerosols. Throughout the atmospheric chemistry processes, the positive feedback between aerosol and water vapor was ubiquitous. For example, hygroscopic processes of anthropogenic secondary inorganic resulted in abundance of aerosol liquid water content (Wu et al., 2018), and the latter of which could provide an efficient media of multiphase reaction which promote new particle formation, and so on. Therefore, the particles in $PM_{2.5}$ generally approach to spherical in shape, resulted in a low δ value, and the high RH and the high possibility that spherical particles formed. The morphological changes of particles in $PM_{2.5}$ could be well simulated on the basis of T-matrix method (Pan et al., 2017).

11

For mineral dust particles, as discussed, the $\delta_{Dp=5}$ value (0.3~0.5) was clearly higher than that of particle in fine mode (Figure 8b). Since the mass concentration of cSO4 and cNH4 were insignificant in coarse mode, the $\delta_{Dp=5}$ value was plotted versus mass fraction of cNO3 in PM2.5-10. Decrease of δ value of dust particles as a function of mass fraction of cNO3 in PM2.5-10 was also obvious, especially when RH was high than 60%. Numbers of studies have reported emission of anthropogenic dust in NCP was significant, and calcium was the most abundant crustal element in NCP. We believed that that Ca(NO3)2 present on the surface of mineral dust particles, and the decrease of $\delta_{Dp=5}$ value of particle in coarse mode was mostly due to heterogeneous reactions and consecutive water-absorbing processes. Such kind of mineral dust particles coated with anthropogenic pollutants have been observed by numbers of previous electro-microscopic studies. Previous studies (Reitz et al., 2011;Gu et al., 2017;Ma et al., 2013) also demonstrated the presence of cSO4 on the surface of dust particles, nevertheless, we think the effect of cSO4 on the decrease of $\delta_{Dp=5}$ value was negligible because the mass fraction of cSO4 was tiny (<0.02) and the CaSO4 was hard to dissolve in limited amount of aerosol liquid water content. To note that, the chemical compounds (such as kaolinite, illite, humic matters, etc.) of particles in coarse mode was very complicated, $\delta_{Dp=5}$ value just indicate a synthetically effect of morphological changes as a result of all physical and chemical processes. To quantitatively characterize their optical and environmental effect, detailed studies on $\delta_{Dp=5}$ value variability of one-fold compound in the laboratory was still essentially need.

4 Conclusions and implications

Depolarization properties of aerosol particles is an important parameter classifying the aerosol types and describing the variability of morphology of particles, which is affected by complicated mixing processes and heterogeneous reactions. It also has great impact on its transport and regional/global climate due to alteration of optical properties of particles. In 2017, a field joint campaign (In-depth study of air pollution sources and processes within Beijing and its surrounding region, APHH-Beijing) was performed at an urban site in Beijing mega city. One of key aims of the project is to assess the processes by which pollutants are transformed through atmospheric chemical reactions. Taking this opportunity, we performed an online observation on the depolarization ratio of single particles using a Polarization Optical Particle Counter. The chemical compositions (SO_4^{2-}, NO_3^-, WSOC) and acidity of particles in both fine mode (PM2.5) and coarse mode (PM2.5-10) was determined using a continuous dichotomous Aerosol Chemical Speciation Analyzer (ACSA-14). The main conclusions are as follows: (1) Depolarization ratio (δ) of ambient particles generally increase with its size due to increase in irregularity of the particles, and the characteristic values of δ for the particles at Dp = 1 μm and 2 μm were 0.11, 017, respectively. Once the observation site was influenced by dust event, both of δ values increased to above 0.3 due to presence of submicron mineral dust particle in irregular shape. The δ value of the particles at Dp = 2 μm was mainly determined by the mass fraction of water-soluble inorganic matter in PM2.5, in which water vapor was fully involved in their atmospheric formation processes. (2) In NCP, anthropogenic dust was an important contributor to the atmospheric loading of particles, their δ values (0.2-0.3) were found to be smaller than that (0.5) of nature dust because of adsorption of acidic substance (such as HNO3) and coagulation with water-soluble anthropogenic pollutants (nitrate, sulfate) and consecutive chemical reactions on the surface of dust.

Ambient relative humidity plays a key role in altering the morphology of mineral dust as a result of hygroscopic processes of deliquescent substances such as $Ca(NO_3)_2$, in particular when RH > 80%. In this study, we found that δ values of mineral dust particle in NCP could be as smaller as 0.2, which could be termed as "quasi-spherical". (3) We found that allocation of anthropogenic pollutants in fine and coarse mode was influenced by the RH along the trajectories of air mass, and increase of nitrate mass in coarse mode was highly associated with the dust event. It indicated that the mineral dust particles in NCP was mostly coated with anthropogenic pollution, upon which classification and quantitative determination of anthropogenic dust emission was possible, though a pioneering study have been done on the basis of satellite remote sensing and land type (Huang et al., 2015).

In this study, we provided solid evidences in morphological changes of mineral dust particles in NCP. Variability of δ value of particles is also a valuable parameter in distinguishing how mineral dust particle interacted with anthropogenic pollutants in formation of regional-scale haze pollutions. This result also spurs us to revisit decades of Lidar observation data in better describing the transport and vertical distribution of Asian dust and pollution, and its regional environmental effects under the scenarios of China thirty years' rapid urbanizations. A reliable optical model capable of discriminating multiple aerosol types was necessary for detailed analysis of polarization-related remote sensing observations. This study suggested that an integrated observation network with single-particle-based depolarization measurement was necessary for synthetically understanding chemo-physical properties of Asian dust issue.

References

Gu, W., Li, Y., Zhu, J.-x., Jia, X., Lin, Q., Zhang, G., Ding, X., Song, W., Bi, X., Wang, X., and Tang, M.: Investigation of water adsorption and hygroscopicity of atmospherically relevant particles using a commercial vapor sorption analyzer, 3821-3832 pp., 2017.

Hara, Y., Yumimoto, K., Uno, I., Shimizu, A., Sugimoto, N., Liu, Z., and Winker, D. M.: Asian dust outflow in the PBL and free atmosphere retrieved by NASA CALIPSO and an assimilated dust transport model, Atmospheric Chemistry and Physics Discussions, 8, 8715-8742, 2008.

Hara, Y., Nishizawa, T., Sugimoto, N., Matsui, I., Pan, X., Kobayashi, H., Osada, K., and Uno, I.: Optical properties of mixed aerosol layers over Japan derived with multi-wavelength Mie–Raman lidar system, Journal of Quantitative Spectroscopy and Radiative Transfer, 188, 20-27, http://dx.doi.org/10.1016/j.jqsrt.2016.06.038, 2017.

He, H., Wang, Y., Ma, Q., Ma, J., Chu, B., Ji, D., Tang, G., Liu, C., Zhang, H., and Hao, J.: Mineral dust and NOx promote the conversion of SO2 to sulfate in heavy pollution days, Sci Rep, 4, 4172, 10.1038/srep04172, 2014.

13

Huang, J. P., Liu, J. J., Chen, B., and Nasiri, S. L.: Detection of anthropogenic dust using CALIPSO lidar measurements, Atmospheric Chemistry and Physics, 15, 11653-11665, 2015.

Kaufman, Y. J., Tanre, D., and Boucher, O.: A satellite view of aerosols in the climate system, Nature, 419, 215-223, 10.1038/nature01091, 2002.

Kim, J.-S., and Park, K.: Atmospheric aging of Asian dust particles during long range transport, Aerosol Science and Technology, 46, 913-924, 2012.

Kimoto, H., Ueda, A., Tsujimoto, K., Mitani, Y., and Kimoto, T.: Development of a Continuous Dichotomous Aerosol Chemical Speciation Analyzer, Clean Technology, 23, 49-52, 2013.

Kobayashi, H., Hayashi, M., Shiraishi, K., Nakura, Y., Enomoto, T., Miura, K., Takahashi, H., Igarashi, Y., Naoe, H., and Kaneyasu, N.: Development of a polarization optical particle counter capable of aerosol type classification, Atmos Environ, 97, 486-492, 2014.

Krueger, B. J., Grassian, V. H., Laskin, A., and Cowin, J. P.: The transformation of solid atmospheric particles into liquid droplets through heterogeneous chemistry: Laboratory insights into the processing of calcium containing mineral dust aerosol in the troposphere, Geophysical Research Letters, 30, doi:10.1029/2002GL016563, 2003.

Laskin, A., Iedema, M. J., Ichkovich, A., Graber, E. R., Taraniuk, I., and Rudich, Y.: Direct observation of completely processed calcium carbonate dust particles, Faraday Discuss, 130, 453-468; discussion 491-517, 519-424, 10.1039/b417366j, 2005.

Li, R., Hu, Y., Li, L., Fu, H., and Chen, J.: Real-time aerosol optical properties, morphology and mixing states under clear, haze and fog episodes in the summer of urban Beijing, Atmos Chem Phys, 17, 5079-5093, 10.5194/acp-17-5079-2017, 2017.

Li, W. J., and Shao, L. Y.: Observation of nitrate coatings on atmospheric mineral dust particles, Atmos Chem Phys, 9, 1863-1871, DOI 10.5194/acp-9-1863-2009, 2009.

Ma, Q., He, H., Liu, Y., Liu, C., and Grassian, V. H.: Heterogeneous and multiphase formation pathways of gypsum in the atmosphere, Physical Chemistry Chemical Physics, 15, 19196-19204, 10.1039/C3CP53424C, 2013.

Nie, W., Ding, A., Wang, T., Kerminen, V. M., George, C., Xue, L., Wang, W., Zhang, Q., Petaja, T., Qi, X., Gao, X., Wang, X., Yang, X., Fu, C., and Kulmala, M.: Polluted dust promotes new particle formation and growth, Sci Rep, 4, 6634, 10.1038/srep06634, 2014.

Nishizawa, T., Okamoto, H., Sugimoto, N., Matsui, I., Shimizu, A., and Aoki, K.: An algorithm that retrieves aerosol properties from dual-wavelength polarized lidar measurements, Journal of Geophysical Research: Atmospheres, 112, 2007.

Nishizawa, T., Sugimoto, N., Matsui, I., Shimizu, A., and Okamoto, H.: Algorithms to retrieve optical properties of three component aerosols from two-wavelength backscatter and one-wavelength polarization lidar measurements considering nonsphericity of dust, Journal of Quantitative Spectroscopy and Radiative Transfer, 112, 254-267, https://doi.org/10.1016/j.jqsrt.2010.06.002, 2011.

Nishizawa, T., Sugimoto, N., Matsui, I., Shimizu, A., Hara, Y., Itsushi, U., Yasunaga, K., Kudo, R., and Kim, S.-W.: Ground-based network observation using Mie–Raman lidars and multi-wavelength Raman lidars and algorithm to retrieve distributions of aerosol components, Journal of Quantitative Spectroscopy and Radiative Transfer, 188, 79-93, http://dx.doi.org/10.1016/j.jqsrt.2016.06.031, 2017.

Pan, X., Uno, I., Hara, Y., Kuribayashi, M., Kobayashi, H., Sugimoto, N., Yamamoto, S., Shimohara, T., and Wang, Z.: Observation of the simultaneous transport of Asian mineral dust aerosols with anthropogenic pollutants using a POPC during a long-lasting dust event in late spring 2014, Geophysical Research Letters, 42, 1593-1598, 10.1002/2014gl062491, 2015.

Pan, X., Uno, I., Wang, Z., Nishizawa, T., Sugimoto, N., Yamamoto, S., Kobayashi, H., Sun, Y., Fu, P., Tang, X., and Wang, Z.: Real-time observational evidence of changing Asian dust morphology with the mixing of heavy anthropogenic pollution, Sci Rep, 7, 335, 10.1038/s41598-017-00444-w, 2017.

Pan, X. L., Uno, I., Hara, Y., Osada, K., Yamamoto, S., Wang, Z., Sugimoto, N., Kobayashi, H., and Wang, Z. F.: Polarization properties of aerosol particles over western Japan: classification, seasonal variation, and implications for air quality, Atmos Chem Phys, 16, 9863-9873, 10.5194/acp-16-9863-2016, 2016.

Ramanathan, V., Crutzen, P. J., Kiehl, J. T., and Rosenfeld, D.: Aerosols, climate, and the hydrological cycle, Science, 294, 2119-2124, 10.1126/science.1064034, 2001.

Reitz, P., Spindler, C., Mentel, T. F., Poulain, L., Wex, H., Mildenberger, K., Niedermeier, D., Hartmann, S., Clauss, T., Stratmann, F., Sullivan, R. C., DeMott, P. J., Petters, M. D., Sierau, B., and Schneider, J.: Surface modification of mineral dust particles by sulphuric acid processing: implications for ice nucleation abilities, Atmos. Chem. Phys., 11, 7839-7858, 10.5194/acp-11-7839-2011, 2011.

Shimizu, A., Sugimoto, N., Matsui, I., Arao, K., Uno, I., Murayama, T., Kagawa, N., Aoki, K., Uchiyama, A., and Yamazaki, A.: Continuous observations of Asian dust and other aerosols by polarization lidars in China and Japan during ACE-Asia, Journal of Geophysical Research-Atmospheres, 109, 10.1029/2002jd003253, 2004.

Shimizu, A., Nishizawa, T., Jin, Y., Kim, S.-W., Wang, Z., Batdorj, D., and Sugimoto, N.: Evolution of a lidar network for tropospheric aerosol detection in East Asia, Optical Engineering, 56, 031219, 10.1117/1.oe.56.3.031219, 2016.

Shimizu, A., Nishizawa, T., Jin, Y., Kim, S.-W., Wang, Z., Batdorj, D., and Sugimoto, N.: Evolution of a lidar network for tropospheric aerosol detection in East Asia, Optical Engineering, 56, 031219-031219, 2017.

Sugimoto, N., Matsui, I., Shimizu, A., Uno, I., Asai, K., Endoh, T., and Nakajima, T.: Observation of dust and anthropogenic aerosol plumes in the northwest Pacific with a two-wavelength polarization lidar on board the research vessel Mirai, Geophysical Research Letters, 29, 2002.

Sullivan, R., J. K. Moore, M., D. Petters, M., Kreidenweis, S., C. Roberts, G., and Prather, K.: Effect of chemical mixing state on the hygroscopicity and cloud nucleation properties of calcium mineral dust particles, 2009.

Sullivan, R. C., Guazzotti, S. A., Sodeman, D. A., and Prather, K. A.: Direct observations of the atmospheric processing of Asian mineral dust, Atmospheric Chemistry and Physics, 7, 1213-1236, 2007.

Tang, M., Cziczo, D. J., and Grassian, V. H.: Interactions of Water with Mineral Dust Aerosol: Water Adsorption, Hygroscopicity, Cloud Condensation, and Ice Nucleation, Chemical Reviews, 116, 4205-4259, 10.1021/acs.chemrev.5b00529, 2016.

Tang, M. J., Whitehead, J., Davidson, N. M., Pope, F. D., Alfarra, M. R., McFiggans, G., and Kalberer, M.: Cloud condensation nucleation activities of calcium carbonate and its atmospheric ageing products, Physical Chemistry Chemical Physics, 17, 32194-32203, 10.1039/C5CP03795F, 2015.

Tobo, Y., Zhang, D., Matsuki, A., and Iwasaka, Y.: Asian dust particles converted into aqueous droplets under remote marine atmospheric conditions, Proc Natl Acad Sci U S A, 107, 17905-17910, 10.1073/pnas.1008235107, 2010.

Uno, I., Yumimoto, K., Shimizu, A., Hara, Y., Sugimoto, N., Wang, Z., Liu, Z., and Winker, D. M.: 3D structure of Asian dust transport revealed by CALIPSO lidar and a 4DVAR dust model, Geophysical Research Letters, 35, 2008.

Uno, I., Eguchi, K., Yumimoto, K., Takemura, T., Shimizu, A., Uematsu, M., Liu, Z., Wang, Z., Hara, Y., and Sugimoto, N.: Asian dust transported one full circuit around the globe, Nature Geoscience, 2, 557-560, 2009.

Wang, Z., Pan, X., Uno, I., Li, J., Wang, Z., Chen, X., Fu, P., Yang, T., Kobayashi, H., and Shimizu, A.: Significant impacts of heterogeneous reactions on the chemical composition and mixing state of dust particles: A case study during dust events over northern China, Atmos Environ, 2017.

499 Winker, D. M., Vaughan, M. A., Omar, A., Hu, Y., Powell, K. A., Liu, Z., Hunt, W. H., and Young, S. A.: Overview of the
500   CALIPSO Mission and CALIOP Data Processing Algorithms, Journal of Atmospheric and Oceanic Technology, 26, 2310-
501   2323, 10.1175/2009jtecha1281.1, 2009.

502 Wu, Z., Wang, Y., Tan, T., Zhu, Y., Li, M., Shang, D., Wang, H., Lu, K., Guo, S., Zeng, L., and Zhang, Y.: Aerosol Liquid
503   Water Driven by Anthropogenic Inorganic Salts: Implying Its Key Role in Haze Formation over the North China Plain,
504   Environmental Science & Technology Letters, 5, 160-166, 10.1021/acs.estlett.8b00021, 2018.

505 Zhang, X.-X., Sharratt, B., Liu, L.-Y., Wang, Z.-F., Pan, X.-L., Lei, J.-Q., Wu, S.-X., Huang, S.-Y., Guo, Y.-H., Li, J., Tang,
506   X., Yang, T., Tian, Y., Chen, X.-S., Hao, J.-Q., Zheng, H.-T., Yang, Y.-Y., and Lyu, Y.-L.: East Asian dust storm in May
507   2017: observations, modelling, and its influence on the Asia-Pacific region, Atmos Chem Phys, 18, 8353-8371,
508   10.5194/acp-18-8353-2018, 2018.

509 Zheng, S., Pozzer, A., Cao, C. X., and Lelieveld, J.: Long-term (2001–2012) concentrations of fine particulate matter
510   (PM<sub>2.5</sub>) and the impact on human health in Beijing, China, Atmos Chem Phys, 15, 5715-5725,
511   10.5194/acp-15-5715-2015, 2015.

512

513

514

16
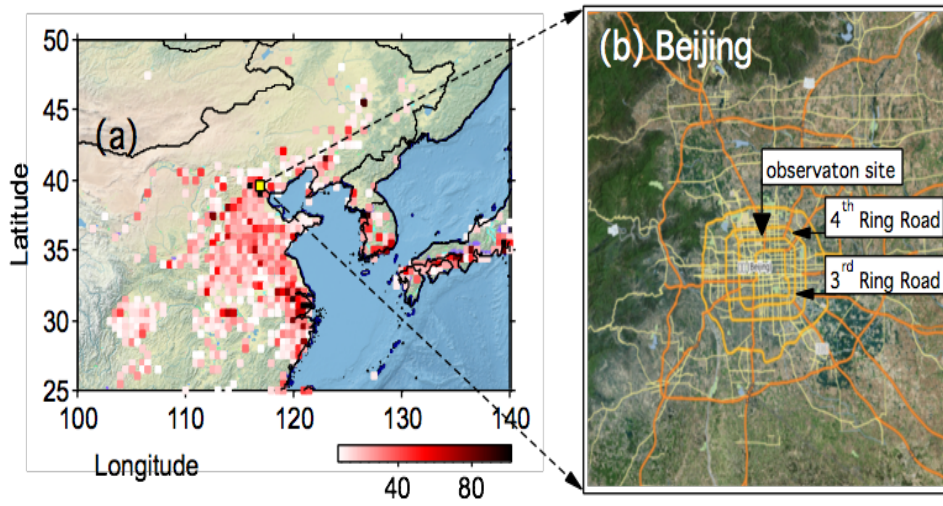
Figures

Figure 1. Geographic location of observation site and NOx emission in East Asia (a), the transportation map of Beijing mega city and location of tower campus of IAP.
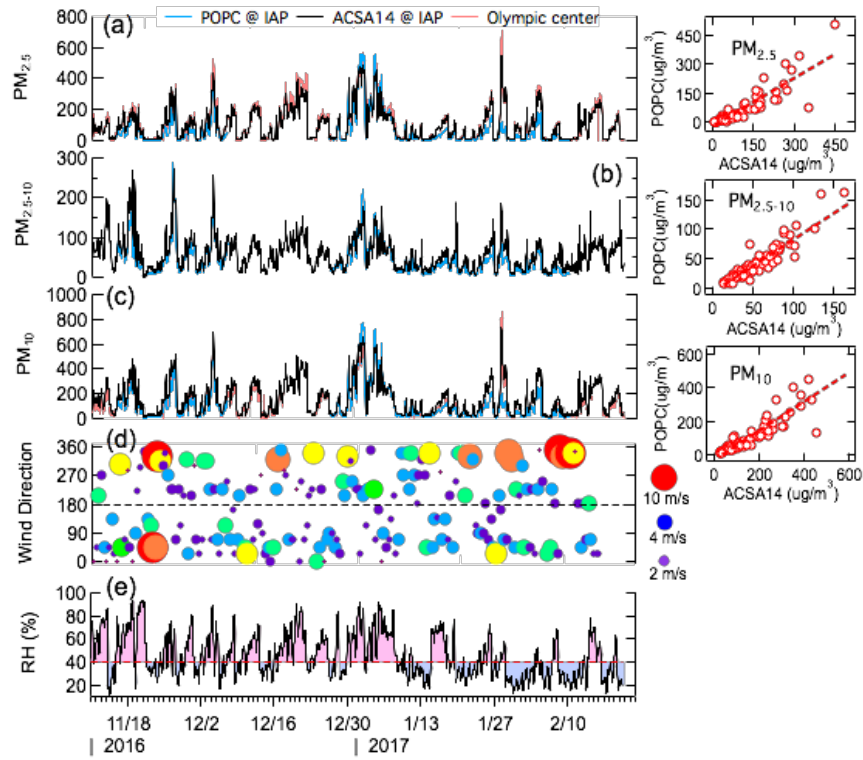
Figure 2. Temporal variation of mass concentration of $PM_{2.5}$ (a), $PM_{2.5-10}$ (b), PM_{10} (c) measured by ACSA14 and derived from POPC measurement, wind speed and direction (d) and relative humidity (e) at observation site. The three scatter plots in the right indicate the linear relationship between ACSA14 and POPC, the correlations are $Y_{POPC} = -6.8 + 0.89 \times X_{ACSA14}$ ($r^2 = 0.86$), $Y_{POPC} = -19.5 + 0.84 \times X_{ACSA14}$ ($r^2 = 0.77$), $Y_{POPC} = -27.7 + 0.87 \times X_{ACSA14}$ ($r^2 = 0.81$) for $PM_{2.5}$, $PM_{2.5-10}$ and PM_{10} respectively.
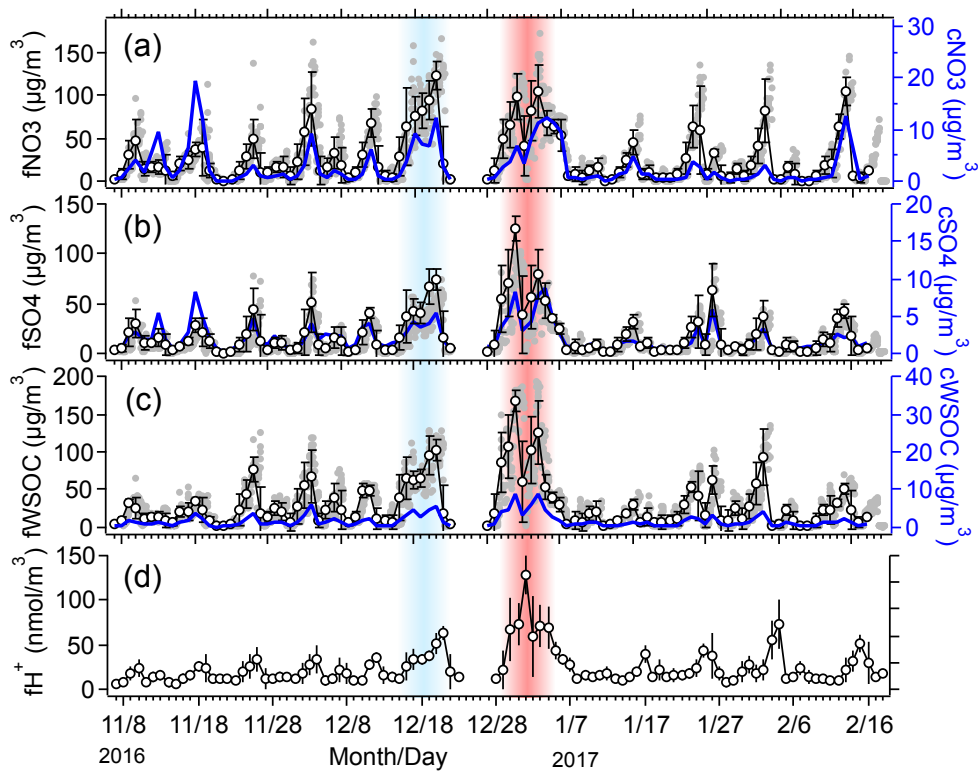
Figure 3 Temporal variations of mass concentrations of nitrate (a), sulfate (b) and water-soluble organic matters (c) in fine mode and coarse mode, and acidity of particle (fH$^+$) in the fine mode (d). Gray dots and white circles represent hourly and daily averaged values on averaged.

19
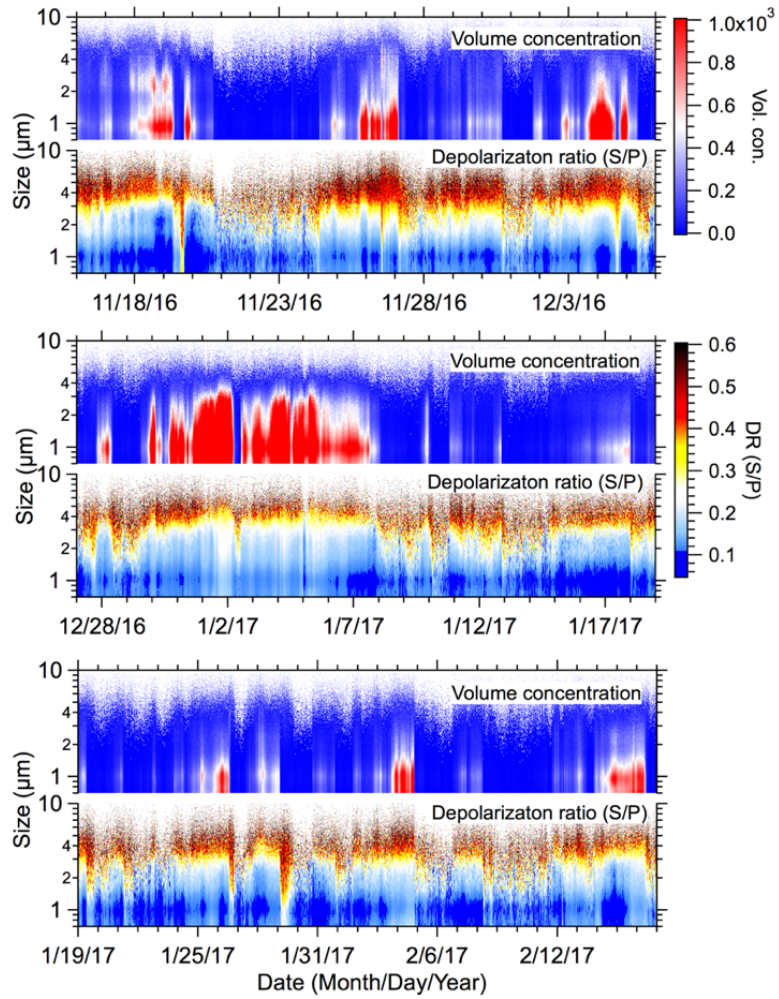
Figure 4 Volume concentrations of particles and corresponding depolarization ratio as a function of time during observation period. For better view the performance of the instrument, the observation results are shown in three-time slots.
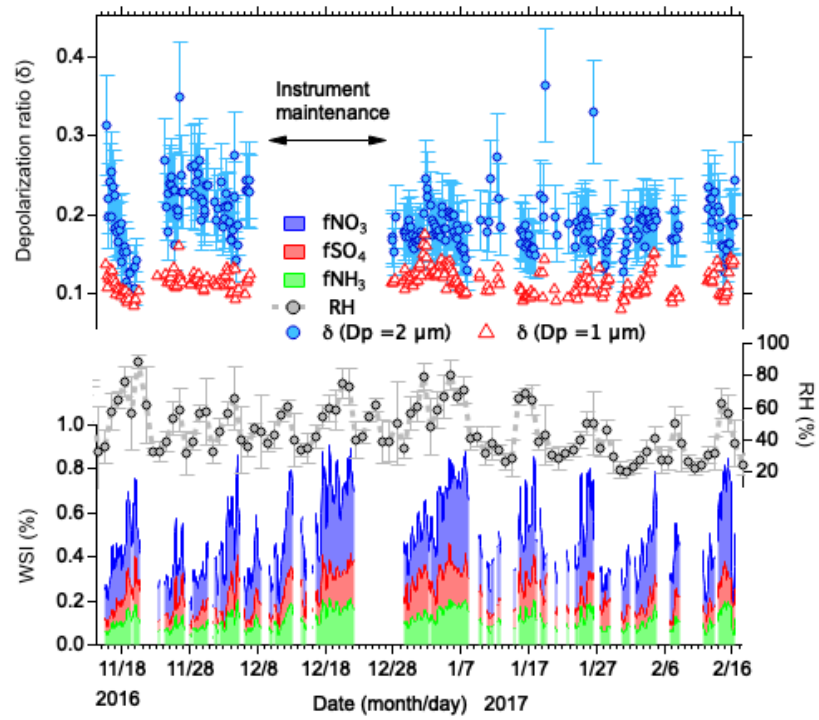
Figure 5 Temporal variabilities of δ value for particles at size of 1 μm and 2 μm (a) and mass fraction of water-soluble inorganic matter (WSI, Blue: nitrate; Red: sulphate; Green: ammonium) in $PM_{2.5}$, ambient RH (b).
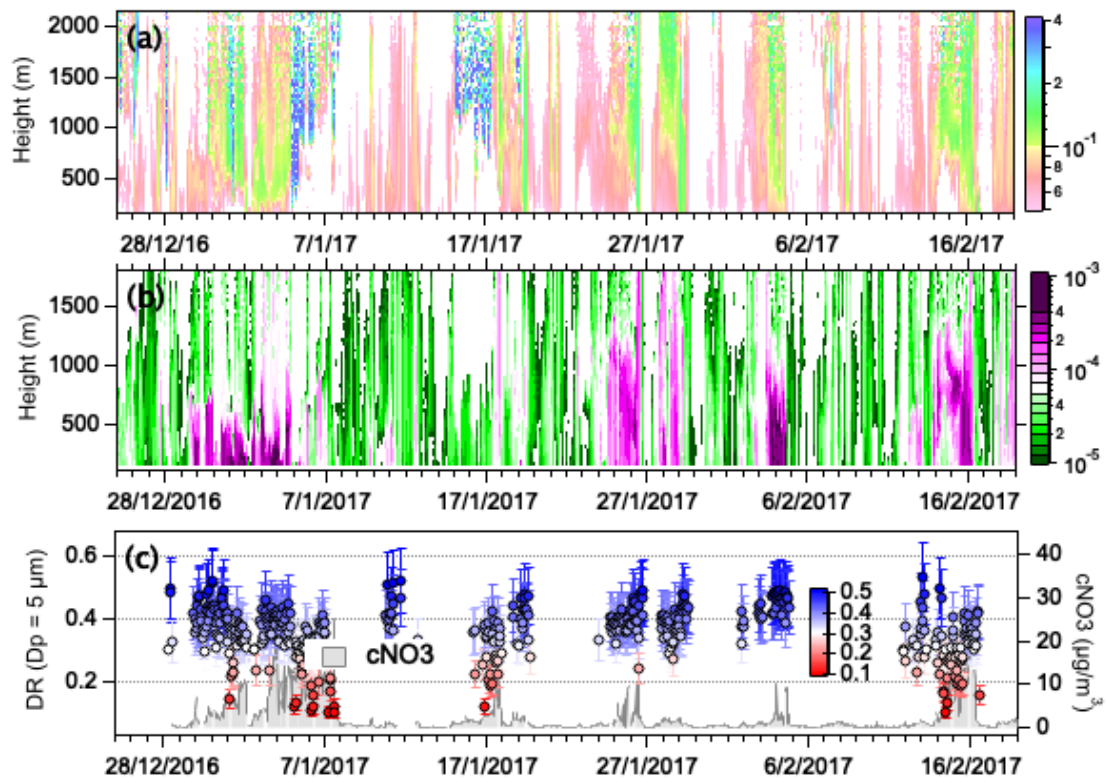
Figure 6 Vertical distribution of volume depolarization ratio (@532 nm) (a), extinction coefficient of dust particles derived from Lidar observation (b) and variability of δ value of mineral dust particles and NO_3^- in coarse mode aerosols (c) as a function of time. Here we choose the particles at a size of 5 μm to indicate the mineral dust particles, marked as $\delta_{Dp=5}$ correspondingly.

22
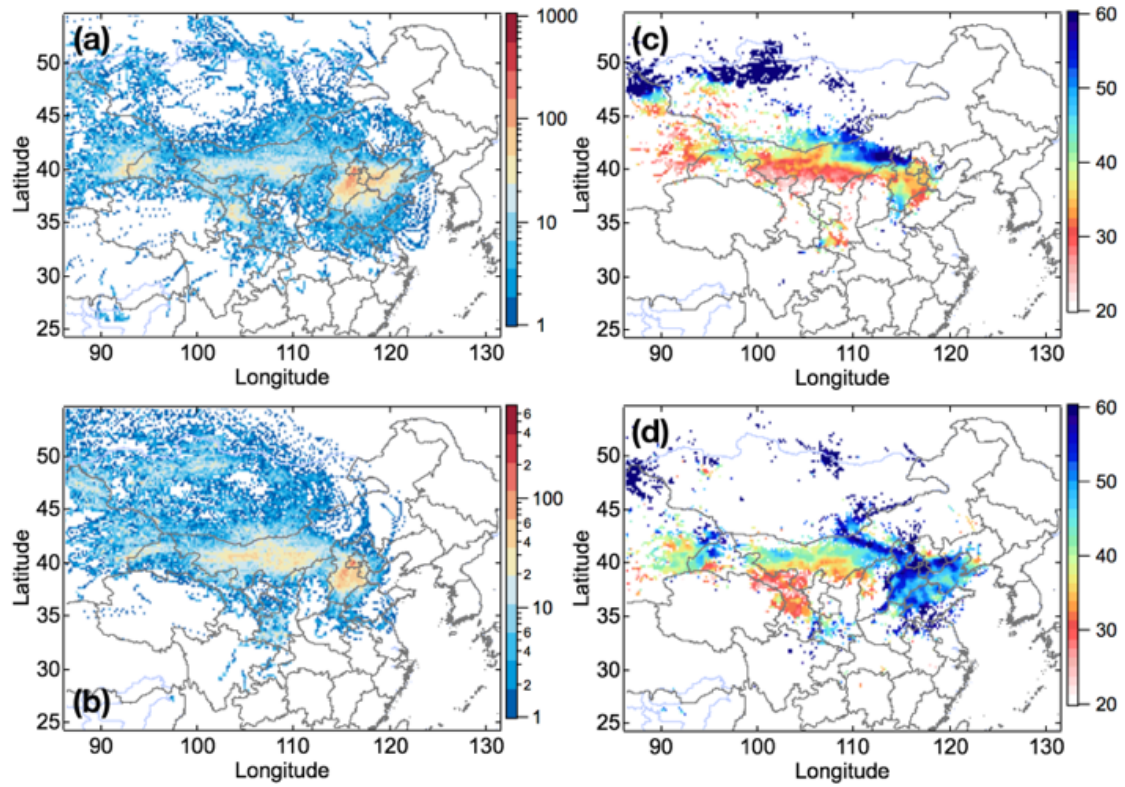
Figure 7 Footprint regions of mineral dust particles for the periods when averaged mass concentration of cNO_3 was higher than 5 µg/m^3, while $\delta_{Dp=5}$ values were higher than 0.4 (a) and lower than 0.2 (b), and corresponding mean RH (c) and (d) in each grid within the footprint area on the basis of ensemble Hysplit analysis. Footprint height was defined as a height that endpoint of backward trajectory was lower than the height of mixing layer in that grid.
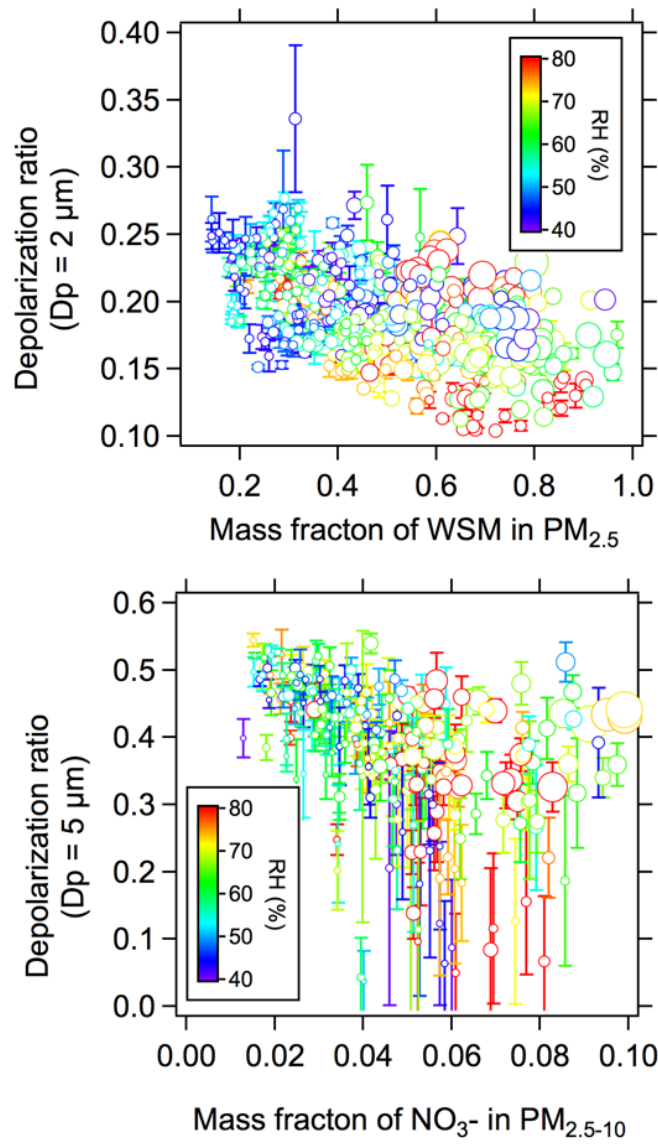
574

575   Figure 8 The variation of $\delta_{Dp=2}$ as a function of mass fraction of WSM in $PM_{2.5}$ (a), and $\delta_{Dp=5}$ as a function of mass fraction of

576   cNO_3 in $PM_{2.5-10}$. The color represents the hourly averaged relative humidity during measurement.

577

578